MICROSTRUCTURAL CHARACTERIZATION OF STONE WOOL FIBRE NETWORK

L. Chapelle[a,b*], P. Brøndsted[b], Y. Kusano[b] , M. R. Foldschack[a]

[a] *Group Research & Development, Rockwool International A/S, Hovedgaden 584, 2640 Hedehusene, Denmark*
[b] *Department of Wind Energy, Section of Composites and Materials Mechanics, Technical University of Denmark, Risø Campus, Frederiksborgvej 39, 4000 Roskilde, Denmark*
**lucie.chapelle@rockwool.com*

Keywords: stone wool, 3D image analysis, x-ray tomography

Abstract
Understanding the mechanical properties of fibrous network as complex as stone wool materials requires a relevant description of their microstructure and architecture. In this study, different methods have been proposed to characterize the fibre orientation, diameter and length of fibres as well as the number density of fibre contacts. The methods are based on image analysis of 3D datasets which have been obtained by x-ray tomography. Validation of the proposed methods was demonstrated by testing generated virtual fibrous network with known fibre characteristics.

1. Introduction

Fibrous materials such as stone wool find applications in the building industry as thermal and acoustic insulators. Previous studies have focused on their thermal and acoustic properties [1-4]. However, other properties such as mechanical strength and durability are also of interest. It is because, for example, during transportation, storage or installation on the construction site, stone wool products are compressed. The macroscopic mechanical properties of stone wool materials are highly influenced by the microstructure such as the fibre network geometry, in particular the orientation distribution of the fibres and the number density of contact points between fibres. Characterization of the microstructure of stone wool is therefore needed to gain an understanding of the macroscopic mechanical properties of stone wool.

X-ray tomography is a powerful tool for the characterization of complex microstructure and their evolution under varying conditions. For instance, porosity content, shape, fibre orientation, diameter, length and tortuosity have been measured and estimated for stone wool by processing and analysing 3D datasets obtained by x-rays tomography [5-8]. Other x-ray tomography experiments involved in-situ loading to observe the strain field during compression of stone wool [9]. Studies have also focussed on detecting fibre contacts. Most of proposed methods consist of extracting the geometrical skeleton of the fibres using a homotopic thinning algorithm. The obtained branches are then classified and merged when belonging to a same fibre [5,10-12]. A method has been proposed in [13] using a local orientation map to detect fibre contacts and then proceed to fibre segmentation.

In this work, we propose methods to estimate the fibre orientation and diameter distribution in a fibrous network where individual fibre segmentation is not a pre-requisite. We also propose a method based on fibre segmentation to find the number of contacts between fibres and determine their length distribution.

2. Materials and methods

2.1 Materials

Stone wool fibres studied are discontinuous glass fibres with a diameter of approximately 3 µm and a length up to a centimetre. They are normally produced by a wheel centrifuge process known as cascade spinning where droplets of melts are drawn into fibres by centrifugal forces. Binder and refined mineral oil are subsequently added to make the material both stable and water repellent. The treated stone wool is then heated in order to cure the binder. The sample chosen for the study is taken from a semi-rigid insulation board commercialized under the name ROCKWOOL Super Flexibatts® with a density of approximately 50 kg/m^3.

2.2 Image Acquisition

Tomography scans were carried out using a high resolution micro-CT system at the Technical University of Denmark (DTU) Imaging Centre. The sample was rotated with an angular increment of 0.1125º. To increase the signal to noise ratio (SNR) of the images, 3200 frames were captured and averaged for each projection on a 2012 x 2012 bit detector array. The 3D image has a size of 1960 x 2012 x 1970 voxels with a voxel size of 0.7964^3 µm^3.

2.3 Fibre orientation

The orientation of the fibres in stone wool was determined using the structure tensor analysis [14]. Let I be the discrete function describing the grey-value intensities of a 3D image and let $p \in \mathbb{R}^3$ be a point belonging to a fibre on I. Because the intensity values along a fibre are locally constant, a vector $v \in \mathbb{R}^3$ exists such that:

$$\big(I(p+v) - I(p)\big)^2 \approx 0 \tag{1}$$

$$|v| = 1 \tag{2}$$

An orientation vector $w(p)$ can be found by setting:

$$w(p) = argmin_{|v|=1}\left(\big(I(p+v) - I(p)\big)^2\right) \tag{3}$$

The expression from equation (1) can be decomposed into a Taylor series:

$$\big(I(p+v) - I(p)\big)^2 \approx \big(v^T \nabla I(p)\big)^2 = v^T \nabla I(p) v^T \nabla I(p) = v^T (\nabla I(p) \nabla I(p)^T) v \tag{4}$$

The minimization problem becomes then:

$$w(p) = argmin_{|v|=1}(v^T (ST) v) \tag{5}$$

where $\boldsymbol{ST} = \boldsymbol{\nabla I(p)\nabla I(p)^T}$ designates the structure tensor.

The orientation vector, *w(p)* is thus the eigenvector corresponding to the smallest eigenvalues of the structure tensor.

The image is first smoothed with an isotropic Gaussian kernel K_ρ of size m_1 and standard deviation ρ. A derivative along each direction *x*, *y* or *z* is computed for each voxel by convolving the image with Sobel-type Sharr operators. The component (J_{ij}) of the structure tensor is expressed as the product of the derivative of the image in the direction *i* with the derivative in the direction *j*, convolved with a second Gaussian filter of kernel size m_2 and standard deviation σ.

$$ST = \begin{bmatrix} J_{xx} & J_{xy} & J_{xz} \\ J_{xy} & J_{yy} & J_{yz} \\ J_{xz} & J_{yz} & J_{zz} \end{bmatrix} where\ J_{ij} = K_\sigma * \left(\frac{\partial (K_\rho * I)}{\partial i} \cdot \frac{\partial I (K_\rho * I)}{\partial j} \right) \tag{6}$$

2.4 Fibre diameter

The size distribution of an object of a set *X* can be assessed through successive openings by a structuring element of growing size. This is referred to as granulometry by openings. For each voxel *p* of an image *I*, we can define the granulometric or pattern spectrum, $PS_{\gamma_n}(p)$ as:

$$\forall\, n > 0, PS_{\gamma_n}(p) = \varphi\left(\psi_n\big(I(p)\big)\right) - \varphi\big(\psi_{n-1}(I(p))\big) \tag{7}$$

where ψ_n is an opening with a structuring element of size *n* and φ is a measure function. For example for a grayscale image, this can simply be the intensity of the voxel. If *X* is the set of fibres and if the structuring element is a ball of radius n, the granulometric curve carries information about the distribution of the diameter of the fibres. The method has mostly been used on binary images. However, during the conversion from grayscale to binary images, some of the information is lost. For example, the voxels corresponding to the edge of the fibre are either set to the background or to the fibre and this will lead to errors in the estimation of the fibre diameter. It is therefore advantageous to work on grayscale images rather than binary.

Commonly, the thickness of the object is then expressed as the scale for which the pattern spectrum reaches its maximal value. However, different maximum values can be reached at different scales. To take into account this effect, we follow the methodology presented in [15]. The expression also includes a scale parameter to correct the bias induced by the edge effect: the intensity of the voxels at the fibre edges reflects the fact that the edges are a mixture of the fibre and the background. Therefore, they should "count" less in the measure of the thickness. The resulting expression for the thickness of a voxel *p* belonging to *I*, $Th(I)(p)$ is given in eq. (8).

$$Th(I)(p) = 2\frac{\sum I(p)\, PS_{\gamma_n}(p)}{\sum PS_{\gamma_n}(p)} - \frac{M - I(p)}{M - m} \tag{8}$$

with *M* and *m* being the maximum and minimum intensities of the image I respectively.

2.5 Number of fibre contacts and fibre segmentation

When the structure tensor is computed for the orientation estimation, and then the eigenvalues and eigenvectors are calculated, another indicator known as the coherency can be extracted from the maximal and minimal eigenvalues, λ_1 and λ_3. The coherency is a measure of how homogeneous the orientation is in a neighbourhood. For a neighbourhood with a preferential orientation (i.e. along a fibre), the coherency value is close to 1. On the other hand, a neighbourhood without a preferential orientation (i.e. the contact zone where a fibre intersects another fibre) results into a value close to 0 for the coherency. The expression for the coherency at a voxel p, $C_t(p)$ is given by:

$$\boldsymbol{C_t(p)} = \left(\frac{\boldsymbol{\lambda_1(p)} - \boldsymbol{\lambda_3(p)}}{\boldsymbol{\lambda_1(p)} + \boldsymbol{\lambda_3(p)}}\right)^2 \tag{9}$$

We compute the coherency for each voxel and threshold the 3D images with this value. The value of the voxels with a coherency value higher than 0.9 is set to zero. As a result, the voxels corresponding to contact zones between fibres with different orientations are removed. We can then proceed to a simple labelling of the fibres based only on the connectivity of the voxels: we consider the 26 neighbours of each voxel and set to the same label all connected voxels. After the thresholding process, the value of the voxels belonging to a fibre where locally the orientation varies abruptly (e.g. fibres extremities) is also set to zero. The last step consists of reconstructing the fibres so that they recover their original shape and volume. We also reconstruct the contact zones and attribute them to the fibres with the lowest label.

2.6 Fibre length

The length of the fibres is extracted from the segmented fibres data: we first calculate the volume of each fibre V_{fib} and then determine the length l knowing the fibre diameter from the local thickness map since we have the following relation:

$$V_{fib} = \int_o^L \pi r^2 dl \tag{10}$$

3. Results and discussion

3.1 Validation using virtual network generation

3.1.1 Virtual network generation

A fibre is modelled as a straight cylinder. Fibres are deposited one by one inside a box. Whenever a fibre intersects with the boundary of the box, the fibre is cut. As the fibre is deposited on top of the previously generated fibres, there is no overlapping of the fibres. The fibre diameter, length and orientation are controlled by statistical distributions (Poisson distribution for the fibre length and uniform distribution for the fibre diameter and orientation). The orientation angle of the fibres is constrained to the *x-y* plane as we expect the real fibre network to tend to have a planar orientation. A visualisation of the generated virtual fibrous network is given in Figure 1.

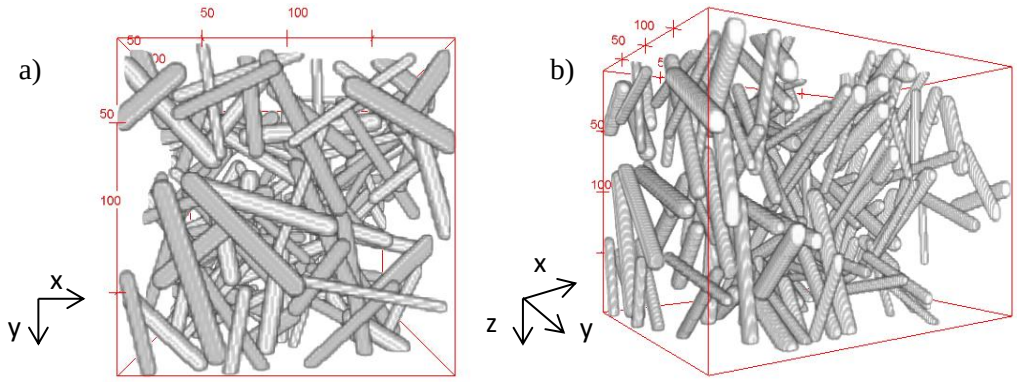

Figure 1. Virtual fibrous network: a) x-y view and b) 3D view

3.1.2 Comparison between input data and data obtained by image analysis

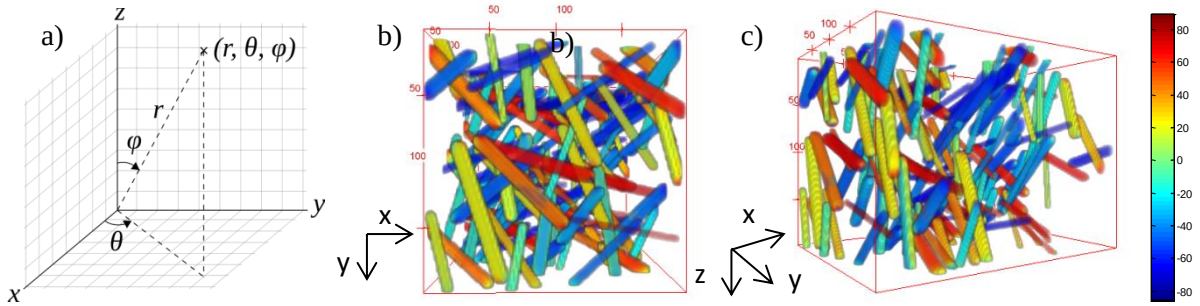

Figure 2. a) Description of the orientation of a point in a 3D space, b) visualization of the fibre orientation of the virtual fibrous network: *x-y* view and c) 3D view (orientation angle in the *x-y* plane is indicated by the colour)

The orientation of a point in 3D can be defined by two angles θ and φ (cf. Figure 2.a). Figures 2.b and 2.c show the estimated orientation of the fibres in the x-y plane (angle θ). We also estimate the orientation angle φ and found as expected a constant value. The graphs of the orientation distribution in the *x-y* plane from Figure 3.a indicate that there is a good correlation between the image analysis measurements and the inputs data from the model. Source of deviation between the real and estimated orientation distribution could be the error in the orientation estimation at the ends of the fibres due to their round shape. We have obtained as well a good agreement between the real and estimated diameter distributions in the virtual fibrous network as presented in the graph of the Figure 3.b.

The contact detection procedure was applied to the virtual fibrous network in order to segment the fibres. Results are shown in Figure 4 where a different colour is randomly allocated to each fibre. Note that that contact zone can be allocated with a different colour than the rest of the fibre. After segmentation, 146 fibres were found instead of 150. The deviation in the results can be attributed to the facts that fibres with similar orientation in contact may not be distinguished (e.g. parallel fibres) and/or that if a fibre has several intersections, it can completely disappear during the thresholding. We could not compare the estimated and input length distribution as fibres are cut during the volume generation process and thus the length is modified automatically.

It is noted that the good correlation between the expected numerical results and the image analysis measurements validate the proposed method for the fibre diameter and orientation as

shown in Figure 3. Regarding the contact detection, fibre segmentation and length measurement, the method leads to reasonable results but will be further improved.

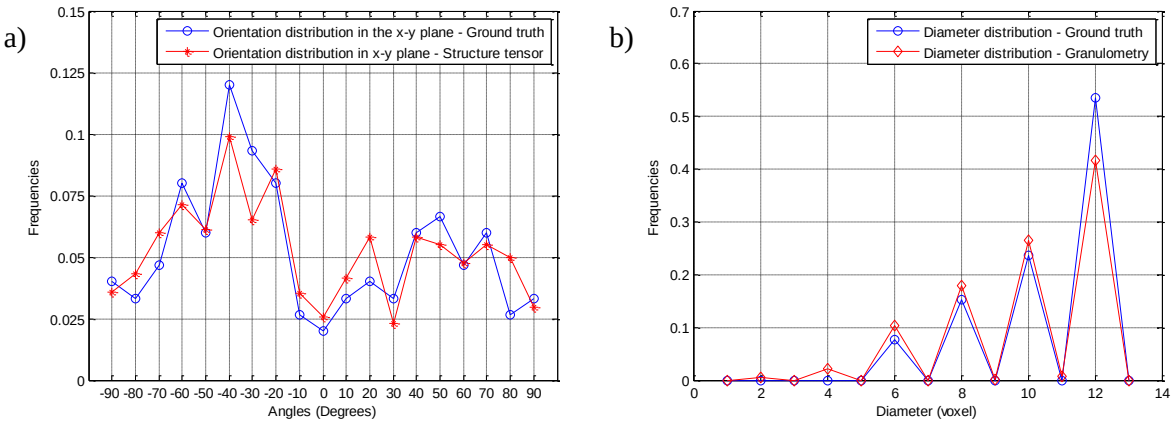

Figure 3. a) Comparison of the real orientation distribution with the estimated orientation distribution and b) of the real diameter distribution with the estimated diameter distribution of the virtual fibrous network.

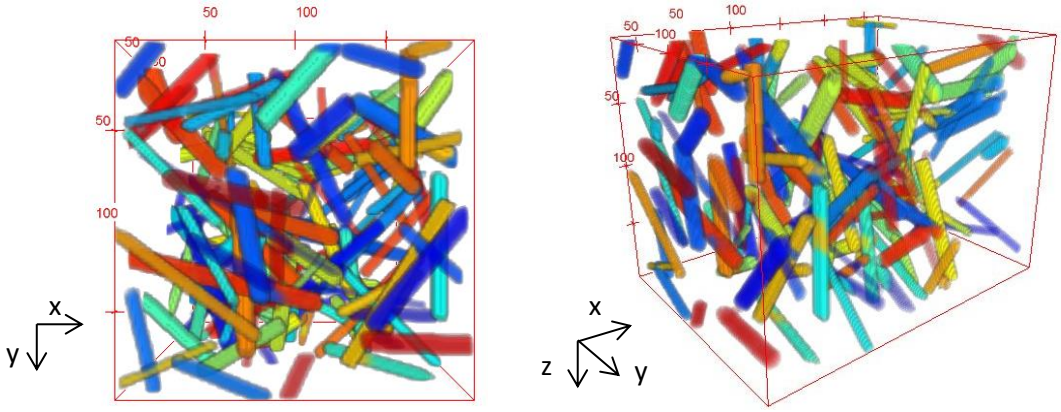

Figure 4. Visualization of the fibre network with random colour allocation for each fibre label

3.2 Real material: stone wool fibre network

In order to reduce the computational effort, only small volumes (400x400x600 voxels) were considered. A visualisation of the volume for the stone wool microstructure is given in Figure 5. The fibres present a wide range of diameters and seem to be oriented quite randomly in the *x-y* plane.

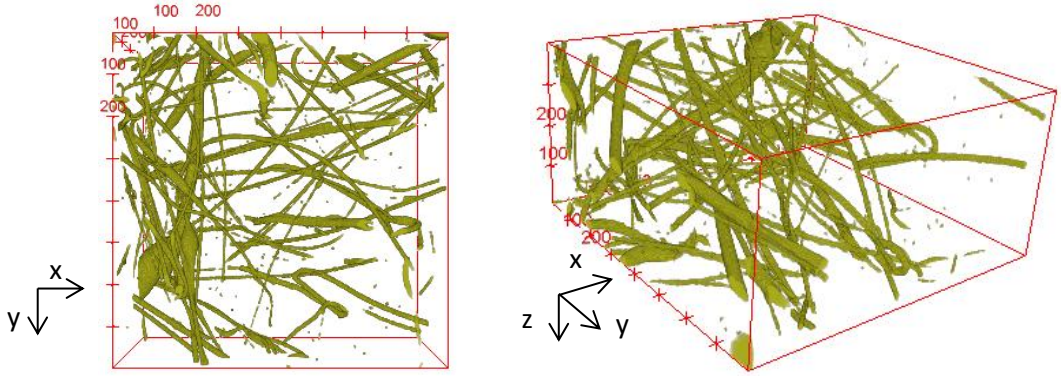

Figure 5. Microstructure of a stone wool sample extracted from a Super flexibatts® product

The results presented in Figure 6.a confirm that the fibres do not show a preferential orientation in the *x-y* plane. Figure 6.b indicates that the orientation φ of the fibres is centred on 40º.

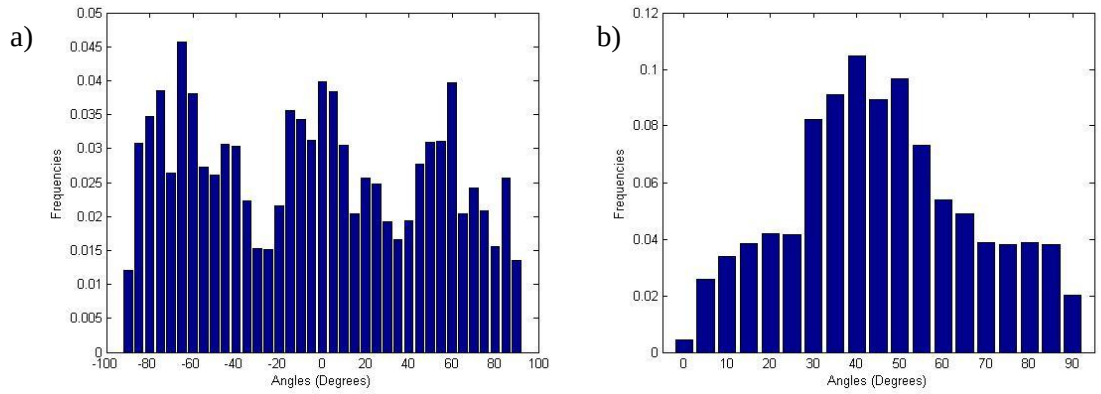

Figure 6. a) Orientation distribution described by the angle θ (*x-y* plane) and b) by the angle φ of a sample taken from a Super flexibatts®

According to the results of Figure 7.2, the fibre radius distribution presents two main peaks centred at 1.4 and 3.3 µm. After segmentation of the fibre network (Figure 7.b), we estimated the number of contacts to be 10 for a total of 121 fibres. We have also estimated the length of each fibre (Figure 7.c), however as the volume considered is really small compared to the length of the fibres, we are only measuring the lengths of fibre segments.

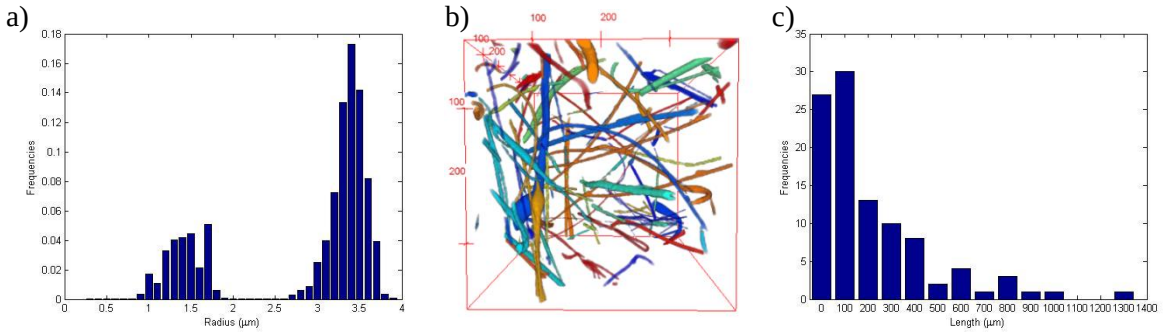

Figure 7. a) Fibre radius distribution and b) fibre segmentation of a sample taken from a Super Flexibatts®

The methods developed in this study have proven to be suitable for the characterization of stone wool microstructure. In order to extract information representative of the material, further studies will be conducted working on larger volume. Fibres are not the only components of stone wool. It also contains shots which are droplets of solidified melt inherent to the fiberization process, and binder. To fully characterize the microstructure of the stone wool product, methods to quantify the binder and the shots distribution are being developed.

4. Conclusion

In this work, we propose methods for characterization of complex fibre networks, such as stone wool, based on image analysis of 3D datasets obtained by x-ray tomography. Estimation of the orientation and diameter of the fibre does not require for preliminary segmentation of the fibres. However, to determine the number of contact points as well as the length of the fibres, we need to first be able to distinguish each fibre. Methods have been validated using a

virtual fibrous network. Once full characterization is achieved, a virtual fibrous network using the real material inputs can be created. An analysis should then be performed in order to determine the minimal achievable size for the volume to be statistically representative of a stone wool product. Finally using this volume as an input in a finite-element analysis, mechanical properties of stone wool will be predicted.

References

[1] F. M. B. Andersen and S. Dyrbøl. Modelling radiative heat transfer in fibrous materials: the use of Planck mean properties compared to spectral and flux-weighted properties. *Journal of Quantitative Spectroscopy and Radiative Transfer*, 60(4):593-603, 1998.

[2] J. Lux, A. Ahmadi, C. Gobbé and C. Delisée. Macroscopic thermal properties of real fibrous materials: Volume averaging method and 3D image analysis, *International Journal of Heat and Mass Transfer*, 29:1958-1973, 2006

[3] C. Peyrega and D. Jeulin. Estimation of acoustic properties and of the representative volume element of random fibrous media, *Journal of Applied Physics*, 113(10):-

[4] C. Jensen and R. Raspet. Thermoacoustic properties of fibrous materials, *Journal of Acoutic Society of America*, 127(6):3470-3484, 2010

[5] J. Lux, C. Delisée and X. Thibault. 3D characterization of wood based fibrous materials: an application, *Image Analysis & Stereology*, 25:25-35, 2006

[6] M. Krause, J. M. Hausherr, B. Burgeth, C. Hermann and W. Krenkel. Determination of the fibre orientation in composites using the structure tensor and local X-ray transform, *Journal of Material Science*, 45:888-896, 2010

[7] H. Altendorf and D. Jeulin. 3D directional mathematical morphology for analysis of fiber orientation, *Image Analysis and Stereology*, 28(3):143-153, 2009

[8] A. Miettinen, C. L. Luengo-Hendriks, G. Chinga-Carrasco, E. K. Gamstedt and M. Kataja. A non-destructive X-ray microtomography approach for measuring fibre length in short-fibre composites, *Composites Science and Technology*,72:1901-1908, 2012

[9] F. Hild, E. Maire, S. Roux and J. F. Witz, Three-dimensional analysis of a compression test on stone wool, *Acta Materialia*, 67(11):3310-3320, 2009

[10] J. P. Masse, L. Salvo, D. Rodney, Y. Bréchet and O. Bouasziz. Influence of relative density on the architecture, and mechanical behaviour of steel metallic wool, *Scripta Materialia*, 54(7):1379-1383, 2006

[11] J. C. Tan, J. A. Elliott and T.W. Clyne. Analysis of tomography images of bonded fibre network to measure distributions of fibre segment length and fibre orientation, *Advanced Engineering Materials*, 8(6):495-500, 2006

[12] H. Yang and B. W. Lindquist, Three-dimensional image analysis of fibrous materials, Proceedings *SPIE 4115*, Applications of Digital Image Processing XXIII, 275, pages 275-282

[13] J. Viguié, P. Latil, L. Orgéas, P. J. J. Dumont, S. Rolland du Roscoat, J.-F. Bloch, C. Marulier and O. Guiraud, Finding fibres and their contacts within 3D images of disordered fibrous media, *Composites Science and Technology*, 89:202-210, 2013

[14] J. Bigun and G. Granlund, Optimal orientation detection of linear symmetry. In *IEEE First International Conference on Computer Vision*, pages 433-438, 1987.

[15] R. Moreno, M. Borga and O. Smedby. Estimation of trabecular thickness in gray-scale through granulometric analysis. In *Conference on Medical Imaging – Image processing*, 8314, 2012